How can pressure distribution be used to identify the stall angle under subsonic flow?

Mustafa Faisal Rana

I. Nomenclature

α	=	angle of attack	C_L	=	coefficient of lift	P	=	static pressure of the region
ρ	=	fluid density	V	=	flow velocity	g	=	acceleration due to gravity
h	=	altitude	L	=	lift force	L	=	wing area
Re	=	Reynolds number	μ	=	dynamic viscosity	l	=	characteristic length
C_P	=	coefficient of pressure	q	=	dynamic pressure	P_∞	=	free stream pressure

II. Introduction

Airplanes are a necessity in the modern transportation sector, used in a variety of cases from carrying human passengers to cargo shipment over long distances. Flight has allowed for long distance travel to become far more reliable and time efficient, enhancing economic development in previously hard-to-reach areas not only through the usage of planes, but UAVs as well. The creation of UAVs and surveillance drones has allowed for monitoring areas and transporting small packages to be made much more economical and efficient. The fundamental behind airplanes relies on the principles of lift. As the aircraft speeds up at an angle, the air around the aircraft begins to move faster, which creates a pressure gradient around the airplane, specifically a region of lower pressure both above and below the wing (with the region above the wing having significantly lower pressure during operation) allowing for lift to generate [1]. The angle at which the aircraft maintains its velocity is highly significant to the lift produced. This angle is known as the angle of attack (α) and is described as the angle between the chord of an aerodynamic body and the direction of air opposing it. Theory dictates that an increase in the angle of attack increases leads to a linear increase in the (C_L) until a point after which lift decreases, called the stall angle [2]. Knowing this angle is crucial to maximize the lift of an aerofoil and increase the efficiency of a plane. It also helps prevent a plane from stalling, which is where C_L begins to decrease and flow separation occurs and moves from the rear to the front of the aerofoil, with turbulent air over the wing and a lack of laminar flow, in turn causing no lift to be generated. The NACA0012 is a symmetrical aerofoil that has a variety of applications. It has a symmetrical shape with a maximum chord thickness of 12%. Some of its applications include their use in unmanned aerial vehicles (UAVs) as they benefit from the NACA0012's stability and predictable performance [3]. This research aims to describe whether a wind tunnel can provide reliable results that would be highly accurate as to what should be expected when the experiment on the NACA0012 would be conducted in real life conditions.

III. Literature Review

The principle of lift in aerodynamics stems from the six following interlinking factors: velocity, density, pressure, temperature, characteristics of the aerofoil and angle of attack. Each of these factors makes a significant contribution to generating lift. The change of oncoming air relative to the airplane is the primary reason for the generation of lift. The act of an aircraft speeding up causes a difference in velocity between the aircraft and the air surrounding the aircraft [4]. The air above the aircraft's wing moves at a faster speed than the air below the wing which results in a pressure difference between the two sides of the wing. Since the air moves out faster over the top side of the wing, it has a lower pressure than the underside of the wing. The lower pressure above creates pressure-induced suction, exerting an upwards force on the aircraft and ultimately, lifting the wing. The α is a key factor when it comes to generating lift. This measures the angle between the relative wind flow and the leading edge of the aerofoil. As this angle increases, C_L also increases, however only till a point, after which the increase in angle of attack does not lead to an increase in C_L and lift generation becomes unpredictable. In 1738, Bernoulli published his principle, which is shown by equation 1

below. This equation related the values of velocity, pressure, fluid density, gravity, and height and compared it between two different fluids. Due to the law of the conservation of energy, the equation states that the energy in one region of the fluid must be the same as the other region of the fluid.

$$P_1 + \frac{1}{2}\rho V_1^2 + \rho g h = P_2 + \frac{1}{2}\rho V_2^2 + \rho g h \tag{1}$$

A. Factors Affecting Lift

Numerous factors affect the generation of lift on an aircraft. These can be separated into three categories: factors that emanate from the aerofoil, factors that emanate from the surrounding air and the Reynolds number.

Each aerofoil has a different series of characteristics, typically defined through their name. As the NACA0012 is investigated in this paper, the key characteristics of this aerofoil are its symmetry, and the large quantity of research conducted on it. The factors affecting lift would be the symmetry of the aerofoil (indicated by the "00" in the name, specifying no camber/curvature in the aerofoil) and the maximum thickness (indicated by the "12" in the name, showing that the maximum thickness at any point in the aerofoil is 12% of the length of the aerofoil). In the case of the NACA 0012, the symmetry ensures that the aerofoil experiences zero camber (no curvature in the aerofoil) as both the top and bottom of the NACA 0012 are identical [5]. The thickness of the aerofoil determines the lift and drag experienced. When thickness is increased, the pressure difference between the top and bottom of the aerofoil is increased as the air on the upper side flows at a higher velocity when the thickness is increased, subsequently increasing lift. As shown by Figure 1, an experiment measuring the effect of chord thickness on the C_L determined that at low angles, a strong correlation can be observed between increasing chord thickness and a higher C_L [6]. The NACA 0012 was also evaluated as an aerofoil with a higher thickness and was consistent with the correlation.

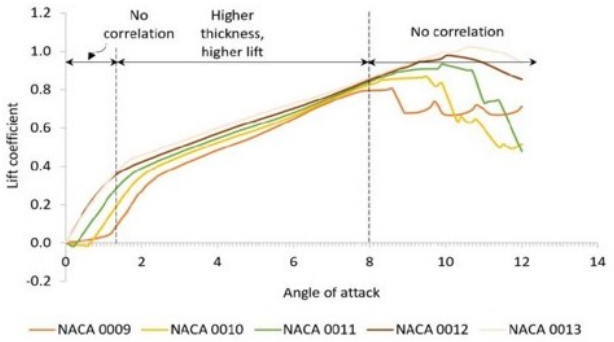


Fig. 1 Effect of increasing chord thickness on C_L [7]

The fluid surrounding the aerofoil has specific characteristics that impact lift in different ways. The observation of this motion can be understood from 2 different perspectives: Eulerian and Lagrangian. The Eulerian perspective looks at fluid flow as a whole at different points in space and time. At these points, the characteristics of flow such as velocity and pressure can be analyzed to gather relevant data regarding what interactions are taking place at the specified location. The Lagrangian perspective on the other hand analyzes different particles within the fluid. These points are tracked throughout the fluid, hence the space analyzed is constantly changing due to the movement of the particle. The Eulerian perspective is applicable in pressure distribution analysis as the pressure along the aerofoil will be analyzed at different points. Hence, the space is fixed and the flow of air over the point will be observed rather than the individual particles. As the Eulerian perspective is observed, there are a number of factors that can be examined which, thereafter, determine lift.

Such factors include density, temperature, dynamic viscosity, velocity, pressure, relative wind flow and humidity. Equation 2below shows the equation of lift. As the fluid density, wing area, and velocity remain constant throughout the experiment, finding the C_L will directly show whether the generation of lift increases. However, it should still be noted that as both velocity and density increase, the lift generated increases as well (density increases lift due to the higher number of air molecules present, which increases the pressure difference between the upper and lower side of the aerofoil, ultimately increasing lift) [8].

$$L = \frac{1}{2}\rho V^2 S C_L \tag{2}$$

The Reynolds number is a non-dimensional quantity used to understand the flow of a fluid and whether it falls under the category of laminar or turbulent flow. The method of calculating the Reynolds number is provided below in equation 3.

$$Re = \frac{\rho V l}{\mu} \tag{3}$$

The equation relates the fluid density, flow velocity, and the dynamic viscosity of the fluid to determine the ratio of inertial to viscous forces. This ratio would then classify the fluid flow as laminar or turbulent. Turbulent flow is a type of flow that is characterized by its changes in pressure and velocity as well as the presence of boundary layer separation and flow disturbances [9]. Laminar flow is a type of flow where fluid motion is smooth and regular and aerodynamic properties (velocity, pressure, etc.) remain constant at every point in the fluid. Turbulent flow prevents lift from generating as the pressure differences are not constant, leading to unpredictable behavior, typically causing a decrease in lift, whilst Laminar flow provides the pressure-induced suction allowing for lift generation. A high Reynolds number would indicate that the flow is turbulent. This number would not only depend on the characteristics of the fluid, but the chord length of the aerofoil as well. Hence, a shorter chord length would lead to a lower Reynolds number, with the opposite being true as well. Turbulent flow prevents lift from generating as the pressure differences are not constant, leading to unpredictable behavior, typically causing a decrease in lift, whilst Laminar flow provides the pressure-induced suction allowing for lift generation. A low Reynolds number would indicate laminar flow, under which C_L increases and the coefficient of drag decreases. Figure 2 shows CFD analysis of the NACA0012 at high Reynolds number. Observing the figure shows that flow separation occurs at the trailing edge of the aerofoil and increases along the aerofoil as the angle of attack increases [10].

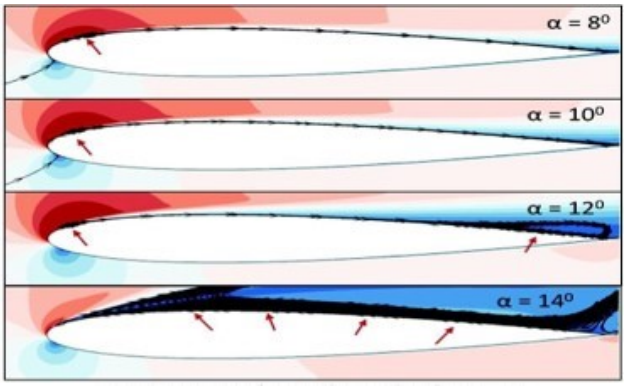


Fig. 2 Flow separation on the NACA0012 [10]

Using equation 3, we can calculate the Reynolds number of the experimental data set to be approximately 23,000. The values inputted for the formula are given in section IV.

B. Principle of Stalling

Stalling is a phenomenon that occurs in aerodynamics where the aerofoil is unable to produce lift anymore as the flow separation point has moved towards the front of the aerofoil [11]. Flow separation is when the fluid above the surface (in this case, the air above the wing/aerofoil) separates from the surface of the object, resulting in an area where the fluid flow becomes turbulent. Figure 3 shows the separation point and the resulting turbulent flow caused by the flow separation from the surface of the aerofoil.

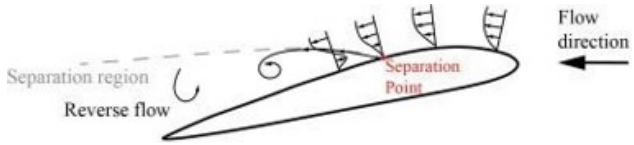


Fig. 3 Flow separation due to high α [12]

The stall angle of an aerofoil is the angle after which the aerofoil stalls and lift generation is severely inhibited. To visualize the stall angle on an aerofoil, the graph of C_L vs angle of attack can be plotted out. By gathering the C_L at different angles, the graph will show the increasing curve of C_L until a point where C_L decreases as the angle of attack increases. This point is known as the stall angle. The highest achieved C_L is known as $C_{L_{max}}$ or the maximum lift coefficient and occurs at the stall angle (as after this, lift generation decreases). Figure 4 shows the change in C_L as angle of attack increases at different Reynolds numbers for the NACA0012 [3]. It can be observed that at a low Reynolds number of 30,000, C_L increases until around an 8-degree incline after which it steadily decreases. The C_L right before the decrease is the $C_{L_{max}}$.

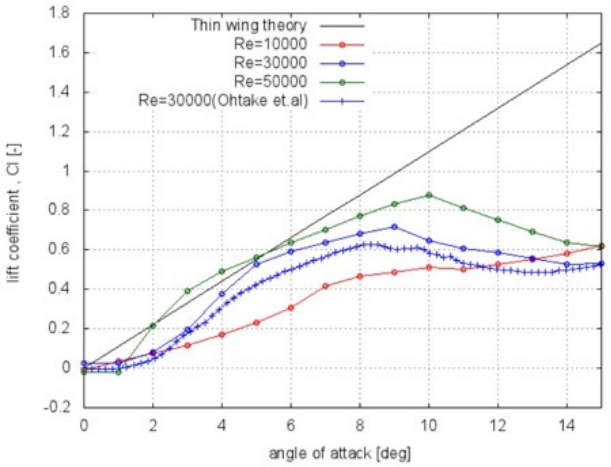


Fig. 4 Graph of C_L vs α for the NACA0012 at different Re [3]

C. Wind Tunnel and Tapping Points

The data regarding the pressure distribution on the NACA 0012 was gathered from an experiment conducted in a wind tunnel. Wind tunnels are facilities developed to mimic flows that an aerodynamic object would interact with during real flight [13]. The object being tested (e.g., the NACA 0012) was placed in the center of the tunnel with controlled air flowing over it. The wind was produced by a fan after which it goes through a turning vane (to turn the direction of the wind) and through a flow straightener and ultimately reaches the testing area. Figure 5 shows a model of a wind tunnel. Different pressure sensors on the aerofoil (known as tapping points) picked up the static pressure at each individual point along the aerofoil and sent these measurements back to the control station. These pressure measurements can be used to calculate the coefficient of pressure (C_P) at each tapping point which will be used to generate a graph of the C_P distribution across the aerofoil at a given angle of attack.

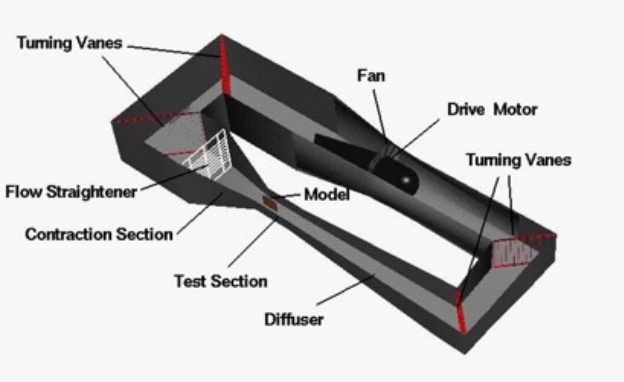


Fig. 5 Labelled wind tunnel [14]

IV. Methodology

Pressure distribution data of the NACA 0012 was taken at a wind tunnel at the University of Nottingham. The wind tunnel had a free stream pressure of −0.31 kPa with a velocity of 20 m s^{-1}. The free stream density was 1.25 kg m^{-3}. There were ten tapping points along the upper surface of the aerofoil and ten tapping points along the lower surface. These tapping points measured the pressure at that point on the aerofoil at 11 different angles of attack (ranging from −2° to 18°, differing by intervals of 2°). Each tapping point's distance from the leading edge of the chord (x) was divided by the chord length (c) (which was 150 mm) to gather a value that gives the relative position of the tapping point along the chord of the aerofoil ($\frac{x}{c}$). Using this data, the dynamic pressure was calculated to be 0.25 kPa (using the formula in equation 4) and will be used for all further C_P calculations. The formula for calculating the C_P is provided below in equation 5 and is used to find the C_P at each tapping point.

$$q = \frac{1}{2}\rho V^2 \tag{4}$$

$$C_P = \frac{P - P_\infty}{q} \tag{5}$$

After calculating the C_P for each tapping point, graphs measuring C_P vs $\frac{x}{c}$ were plotted to see how the C_P changed along the relative position on the chord of the aerofoil. The graph for the C_P at 8° is given below in Figure 6 while graphs for all other angles of attack are provided in the appendix.

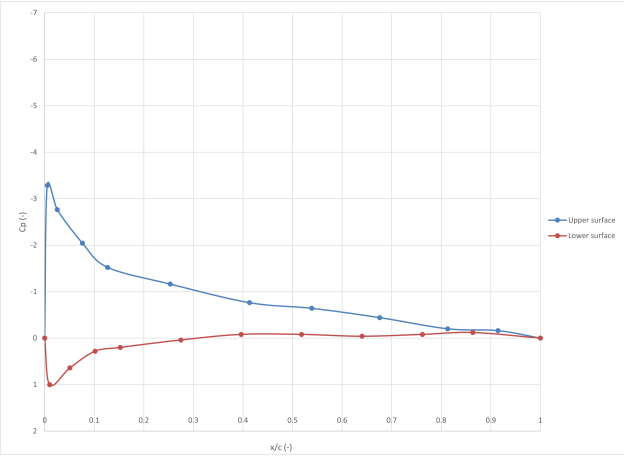


Fig. 6 C_P at 8° against chordwise position

Comparing the graphs in the appendix, a clear increase in the C_P of the upper surface can be observed as the angle of attack is increased. However, figures 18 and 19 have a lower C_P on the upper surface relative to the previous angles of attack. This would show that the stall angle has passed and there is turbulent and unpredictable airflow on the upper surface of the aerofoil, causing a decrease in the C_P. The area under the graph of C_P vs $\frac{x}{c}$ would give the C_L and provide a valid answer as to what angle is the critical angle, what angle has the highest coefficient of lift ($C_{L_{max}}$) and where does the aerofoil undergo stalling. Equation 6 below shows the formula for calculating the C_L.

$$C_L = \frac{1}{c}\int_0^1 (C_{P,lower} - C_{P,upper})dx \tag{6}$$

Using equation 6, C_L for each angle of attack can be found and a graph can be generated that would indicate the angle that has $C_{L_{max}}$ and subsequently the decline in C_L after the angle. Figure 7 below shows the change in C_L as α is increased.

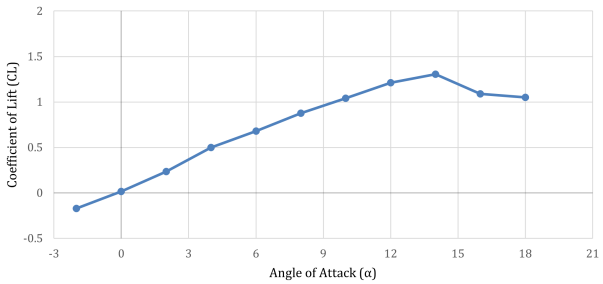


Fig. 7 C_L **vs** α

V. Quantitative Analysis

A. Experimental Data

Observing the graph, it can be noted that as α increases, C_L also increases. This increase only takes place until 14° and the angles succeeding this have a lower C_L than the previous. For this data set, it would indicate that 14° is the stall angle for the NACA0012 as after this point, there is an observable decrease in C_L. $C_{L_{max}}$ would also be present at the stall angle and in this data set, it can be observed to be 1.304. After 14°, the aerofoil undergoes stalling, causing there to be a decrease in lift generation as the flow separation point as moved to the front of the aerofoil, therefore causing a decrease in the C_L. Observing the graph, it should also be noted that the relationship between α and C_L is not linear, even before 14° as the gradient of the graph is inconsistent between each point.

B. Theory Paper

The paper that the experimental data set will be compared to was written in 1973 by N. Gregory and C. L. O'Reilly [15] and is displayed in figure 8. The conditions of the experiment are similar to those in the experimental data set, with both conducting the test at subsonic speeds and in a low-speed wind tunnel. The paper presents a graph for C_L vs α on the NACA at varying Reynolds Numbers (shown below in figure 9), however, only the data gathered at the 2 lowest Reynolds Numbers are analyzed as these are the closest to the Reynolds Number present in the experimental data set. Plotting the data set for these two Reynolds Numbers compared to the experimental data set provides the graph shown in figure 9.

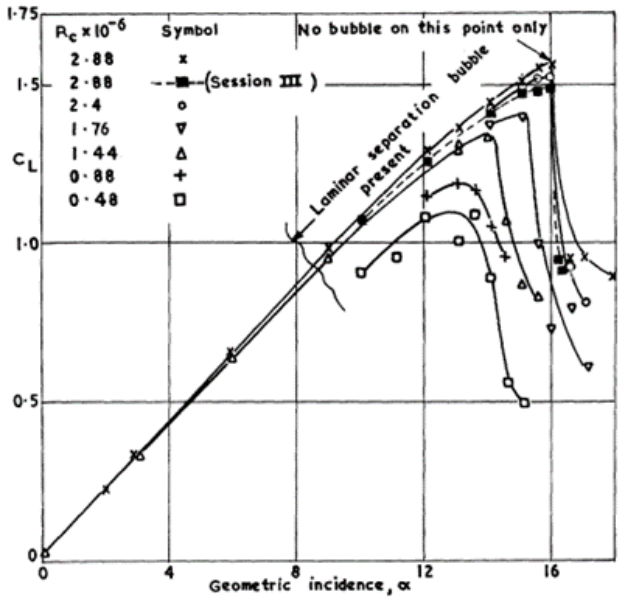


Fig. 8 Theory paper graph showing C_L vs α [15]

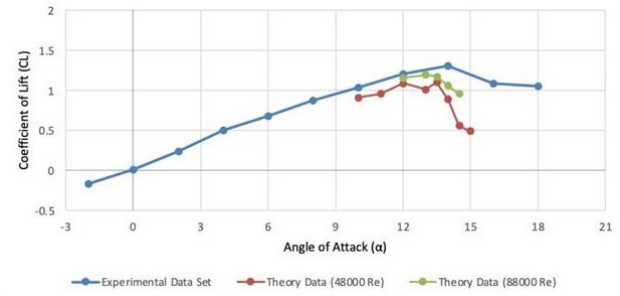


Fig. 9 Experimental dataset vs. theoretical data at Re = 4.8×10^4 and Re = 8.8×10^4

VI. Conclusion

As shown by figure 9, the experimental data sets and theory data sets share similar values for C_L. However, they slightly differ when it comes to the stall angle, with the experimental data set having the stall angle slightly higher than both theory data sets. Numerous reasons can justify this difference; however, the key reason can be the differing Reynolds Numbers. As shown by the 2 data sets acquired from the theory paper, when Reynolds number increased from 48,000 to 88,000 (whilst all other conditions remained constant), the stall angle lowered by approximately 0.5°. As the experimental data set had a Reynolds number of 23,000 it was lower compared to the lowest Reynolds number from the theory paper. Hence, the pattern observed in the theory paper would imply that the stall angle in the experimental data set should be approximately 0.25-0.5° higher compared to that of the 48,000 Re data set. This stands true as when the graph is observed, the experimental data set has a stall angle of 14° compared to the 48,000 Re data sets stall angle of 13.5°.

In summary, measuring the stall angle of the NACA0012 was observed to be 14°, with the $C_{L_{max}}$ at this angle being 1.304. Comparing this to the data sets gathered from the theory paper (which had wind tunnel conditions that were similar to real life conditions), both the theory paper and the experimental data set had very similar results for C_L, with the difference in their stall angle being attributed to the difference in Reynolds Number. Hence, the results from this paper would indicate that a wind tunnel would be able to effectively replicate real-life conditions. It should be noted that the theory paper did not have the same range of α as the experimental data set, hence any changes that the experimental data set and theory paper had from $-2°$ till 10° were unable to be observed. The experimental data set

only took measurements at each consecutive integer value for α, whereas the theory data set had taken measurements at angles such as 13.5° and 14°. This may lead to some inaccuracy when observing the stall angle from the experimental data set. Whilst the theory paper and experimental data set both used subsonic speeds, the theory data sets used a speed of $55\,\mathrm{m\,s^{-1}}$ whereas the experimental data set used $20\,\mathrm{m\,s^{-1}}$, which could lead to differences when calculating q and Re.

Appendix

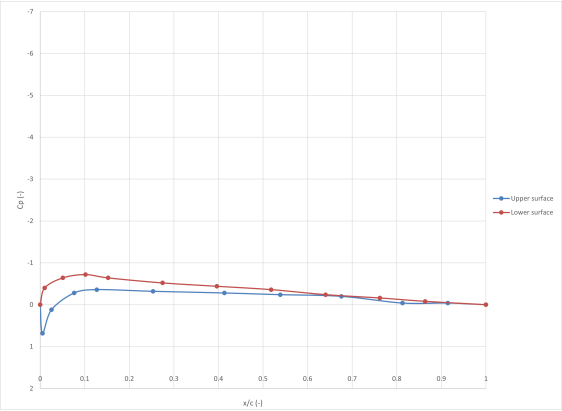


Fig. 10 C_P **at** $-2°$ **against chordwise position**

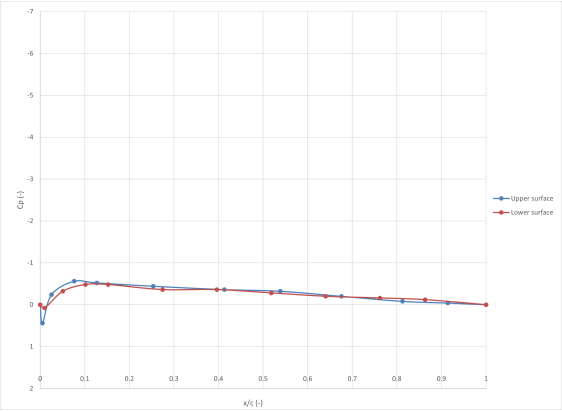


Fig. 11 C_P **at** $0°$ **against chordwise position**

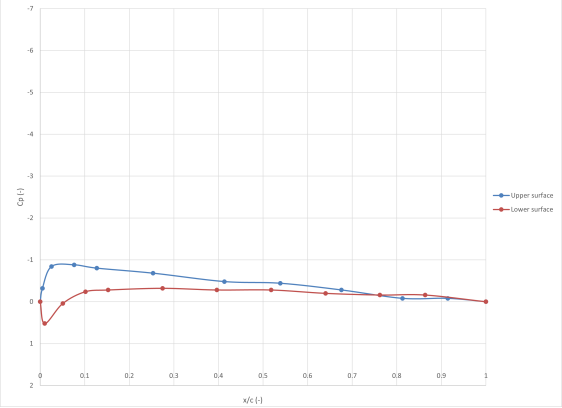


Fig. 12 C_P **at** $2°$ **against chordwise position**

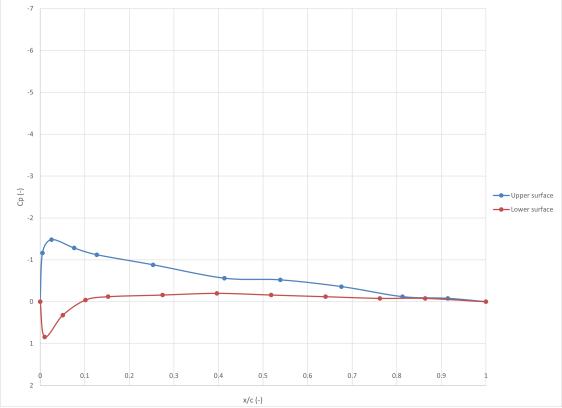


Fig. 13 C_P **at** $4°$ **against chordwise position**

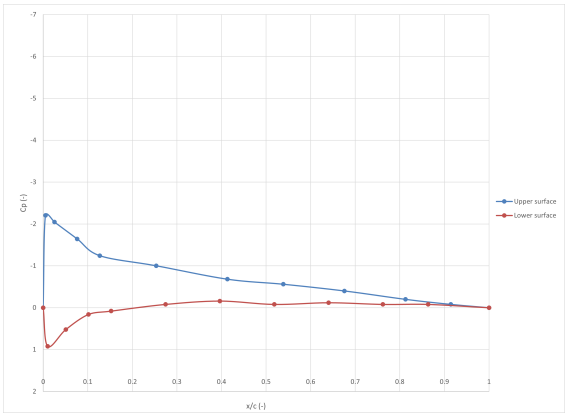


Fig. 14 C_P **at** 6° **against chordwise position**

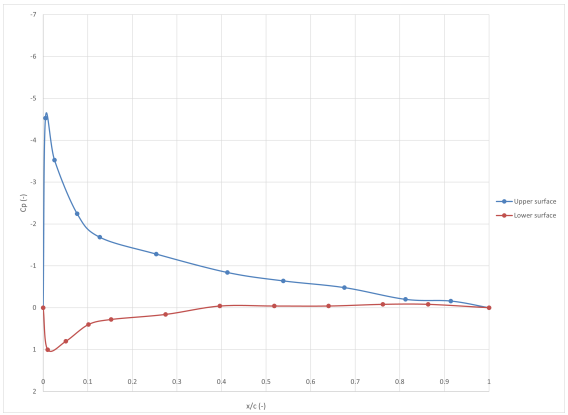


Fig. 15 C_P **at** 10° **against chordwise position**

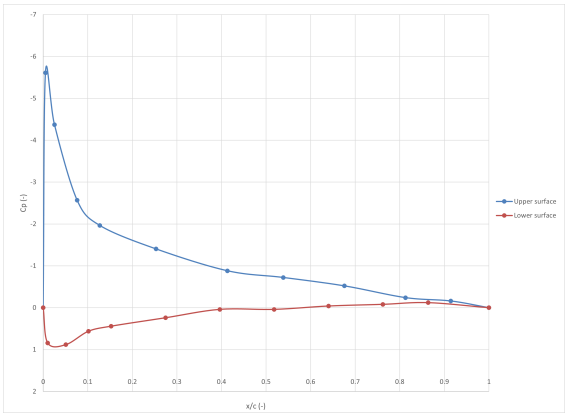


Fig. 16 C_P **at** 12° **against chordwise position**

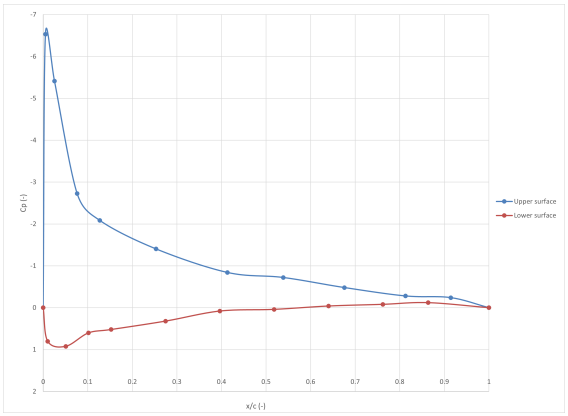


Fig. 17 C_P **at** 14° **against chordwise position**

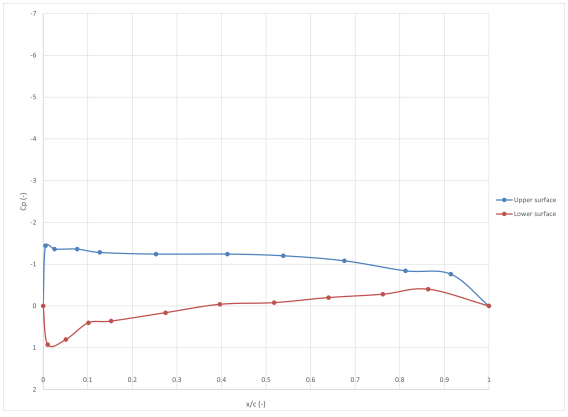


Fig. 18 C_P **at** 16° **against chordwise position**

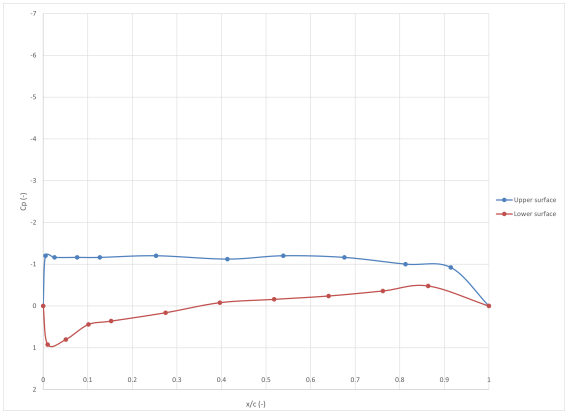


Fig. 19 C_P **at** 18° **against chordwise position**

References

[1] Akbar, A., "Effect Of Angle Of Attack On Airfoil Naca 0012 Performance," *REM (Rekayasa Energi Manufaktur) Jurnal*, Vol. 5, No. 1, 2020, pp. 35–40.

[2] Khalid, M. H., "CFD Analysis of NACA 0012 Aerofoil to Investigate the Effect of Increasing Angle of Attack on Coefficient of Lift and Coefficient of Drag," *Journal of Studies in Science and Engineering*, Vol. 2, No. 1, 2022, pp. 74–86.

[3] Yamaguchi, Y., Ohtake, T., and Muramatsu, A., "Pressure distribution on a NACA0012 airfoil at low Reynolds numbers," *The Proceedings of the International Conference on Jets, Wakes and Separated Flows (The Japan Society of Mechanical Engineers*, Vol. 1201, 2013.

[4] Benson, T., "what is Lift?" Tech. rep., NASA, 2021.

[5] Critzos, C. C., Heyson, H. H., and Boswinkle Jr, R. W., "Aerodynamic characteristics of NACA 0012 airfoil section at angles of attack from 0 degrees to 180 degrees," Tech. rep., NASA, 1955.

[6] Wani, I. N., Bhaskar, B., Raghuwanshi, S. S., Kushwah, N., Agrawal, Y., Kumar, A., Pandey, A., and Ayachit, B., "Design & analysis of NACA 0012 airfoil with circular dent of 30 mm depth on upper surface," *Materials Today: Proceedings*, 2023.

[7] Seeni, A., "A theory on understanding aerodynamic phenomena of airfoils and the significance of airfoil's thickness on lift and drag," *INCAS Bulletin*, Vol. 14, No. 3, 2022, pp. 101–110.

[8] Benson, T., "Density Effects on Aerodynamic Forces," Tech. rep., NASA, 2020.

[9] Ilieva, G. I., "On turbulence and its effects on aerodynamics of flow through turbine stages," *Turbulence modelling approaches: current state, development prospects, applications*, Vol. 143, 2017.

[10] Winslow, J., Otsuka, H., Govindarajan, B., and Chopra, I., "Basic understanding of airfoil characteristics at low Reynolds numbers (10 4–10 5)," *Journal of aircraft*, Vol. 55, No. 3, 2018, pp. 1050–1061.

[11] Leishman, J. G., "Stalling & Spinning," *Introduction to Aerospace Flight Vehicles*, 2023.

[12] Vagnoni, E., "The Reaction Turbines Used in PHES Units and Related Problems," *Encyclopedia of Energy Storage*, 2022.

[13] Reis, M., Falcão Filho, J., and Moraes, L., "The TTP Transonic wind tunnel Mach number uniformity analysis," *Measurement*, Vol. 51, 2014, pp. 356–366.

[14] Hall, N., "Wind Tunnel Parts," Tech. rep., NASA Glenn Research Centre, 2021.

[15] Gregory, N., and O'reilly, C., "Low-speed aerodynamic characteristics of NACA 0012 aerofoil section, including the effects of upper-surface roughness simulating hoar frost," *Cranfield aerade reports*, 1970.